Performance of Unwashed Fine Sea-Sand Concrete: Mechanical Enhancement via Seawater Curing and Thermal Behavior in Mass Structures

Van Trieu Nguyen
Coastal Branch of the Joint Vietnam-Russia Tropical Science and Technology Research Center, Vietnam
vantrieu.xumuk@gmail.com

Van Toan Nguyen
Faculty of Civil Engineering, Industrial University of Ho Chi Minh City, Vietnam
nguyenvantoan@iuh.edu.vn (corresponding author)

Van Minh Mai
Coastal Branch of the Joint Vietnam-Russia Tropical Science and Technology Research Center, Vietnam
minhvmaind@gmail.com

Van Kien Dong
Coastal Branch of the Joint Vietnam-Russia Tropical Science and Technology Research Center, Vietnam
vankien29@gmail.com

Khac Ngoc Ho
Coastal Branch of the Joint Vietnam-Russia Tropical Science and Technology Research Center, Vietnam
hokhacngoc94@gmail.com

Received: 16 December 2025 | Revised: 26 January 2026 | Accepted: 4 February 2026

 DOI: https://doi.org/10.48084/etasr.16978

ABSTRACT

This study evaluates the feasibility of using unwashed fine sea sand (fineness modulus of 1.1 and chloride content of 0.06%) in mass concrete structures, examining the mechanical optimization and thermal safety by integrating 10–30% class F Fly Ash (FA) and 5% Silica Fume (SF) with sulfate-resistant cement. The experimental results show that seawater curing increased compressive strength by up to 5 MPa compared to air curing, due to the acceleration of hydration by marine ions and the moisture-assisted pozzolanic reaction working together. The mixture containing 20% FA and 5% SF (FA20SF5) exhibited an optimal balance of workability and strength. A 500 cm × 200 cm × 120 cm mass concrete block exhibited a maximum core temperature of 60 °C, with the radial thermal gradient remaining below 16 °C and settling within 200 h. These results suggest that, despite the presence of accelerating ions in unwashed sea sand, its thermal behavior remains manageable.

Keywords-compressive strength; mass concrete; sea sand; seawater curing; thermal behavior

I. INTRODUCTION

The decline in river sand reserves due to over-exploitation, increasingly stringent environmental regulations, and rising transportation costs has prompted the search for alternative concrete aggregates [1]. Sea sand is a potential source of material due to its large reserves and the ability to mine it in situ [2, 3]. Traditional risks associated with sea sand, primarily concerning dissolved salts and Cl^-/SO_4^{2-} ions, can be significantly reduced by using binder systems with active mineral additives [4, 5]. FA, SF, Ground Granulated Blast Furnace Slag (GGBFS), and Metakaolin (MK) promote pozzolanic and pore-filling reactions, increasing the ability to "retain" chloride by forming AFm and Friedel's salt phases, which densify the microstructure. This reduces free chloride and limits degradation in a marine environment [6-8]. In

particular, using FA and SF together improves compressive strength and Rapid Chloride Permeability Test (RCPT), which is supported by SEM evidence showing a refined pore structure and denser matrix [9]. When sea sand has a high SiO_2 content and a fineness modulus close to that of river sand, the mineral additive system improves the mechanical properties and durability of concrete, helping it reach or exceed the control strength [10, 11]. For the fine sand group (fineness modulus <1.5) with skewed grain distribution [12, 13], excessive fineness has increased the specific surface area, leading to higher water demand, reduced fluidity, an increased the risk of water separation and segregation, and significant deviations in concrete's mechanical and thermal properties without adjustments to the proportions of the mixture or its additives [14-16]. Thus, fine-to-ultrafine sea sands hinder direct application to structural concrete. Although a few laboratory studies and non-structural applications have been conducted, systematic evaluations at actual construction scales have been lacking [17, 18]. Furthermore, ions in sand/seawater could alter early hydration kinetics, promoting early strength but potentially altering the heat evolution curve and thermal gradient with block size [5, 14, 15]. The interactions between the endogenous heat of hydration, the thermal gradient in the bulk, and the coordinated Cl^{-}–SO_4^{2-} erosion mechanism have not been fully elucidated by long-term, large-scale experimental data. Thus, there are reservations and differences of opinion in the engineering community regarding the safety of using fine sea sand for load-bearing structures [4, 15, 19, 20]. To provide additional large-scale data, the present study examines the mechanical properties and thermal characteristics of mass concrete made with unwashed fine sea sand (FM = 1.1). This gradation is characteristic of plentiful coastal deposits in the study region, and it is representative of an "off-spec" material that requires validation for structural use. Using sulfate-resistant cement, FA, and SF, this study evaluates the mechanical development and hydration heat evolution within a 500 cm × 200 cm × 120 cm block. The objective is to clarify the influence of marine ions on hydration thermodynamics and thermal safety, as well as to validate a sustainable binder strategy that optimizes performance while preventing early-age cracking.

II. EXPERIMENTAL PROGRAM

A. Materials

The mix proportions for the 17 concrete designs used in this study are detailed in Table I. To reduce heat evolution, a commonly used range for mass concrete, FA replacement was varied from 10% to 30% by mass of cement. A constant 5% SF addition was adopted in the SF5 series to enhance early-age strength.

- Binder: The primary binder was sulfate-resistant blended Portland cement (PCB40-MS) with a specific gravity of 2.79 g/cm³, a Blaine specific surface area of 3,600 cm²/g, and a retained content on the 0.09-mm sieve of 0.9%. The cement had initial and final setting times of 160 min and 215 min, respectively. Soundness, as determined by the Le Chatelier method, was 0.5 mm, which is well within the allowable limits. The Sulfur Trioxide (SO_3) content was 1.95%.
- Supplementary Cementitious Materials (SCMs): Class F FA, with a density of 2.225 g/cm³, was used as a partial cement replacement. SF, complying with ASTM C1240, was added, featuring a particle size of less than 0.1 μm.
- Aggregates: The fine aggregate was unwashed, untreated sea sand with a fineness modulus of 1.1, a chloride content of 0.06% by weight, and a density of 2.69 g/cm³. This chloride content is relatively low for a marine-derived aggregate and consistent with the supratidal/upper-beach sampling location, where rainfall infiltration and periodic tidal flushing reduce residual salts in the near-surface layer. Higher salt contents may occur in intertidal or submerged sands. Therefore, this value is representative of the specific batch used in this study. The coarse aggregate was gray crushed stone (1 cm × 2 cm), with a density of 2.751 g/cm³ and a water absorption rate of 0.72%.
- Admixtures: A lignosulfonate-based water reducer was used as a plasticizer to maintain workability, and tap water was utilized for all mixtures.

TABLE I. MIXING PROPORTIONS OF 1 m^3 SEA SAND CONCRETE MIXTURE

ID	CM (kg)	FA (kg)	SF (kg)	Sea sand (kg)	Stone (kg)	Water (kg)	Plasticizer (L)
CM	455			509	1242	192	2.73
FA10	408	45		507	1237	191	2.72
FA20	361	90		505	1232	190	2.71
FA30	315	135		503	1226	189	2.69
FA10SF5	384	45	23	506	1234	190	2.71
FA20SF5	338	90	23	504	1229	190	2.70
FA30SF5	292	135	23	502	1225	189	2.69

B. Evaluation of Fresh Concrete

The consistency of the mixture was quantified using slump values assessed according to ASTM C143/C143M [21]. The initial and final setting times were determined according to the IS 8142 standard. Thermal monitoring of the fresh mix was conducted in accordance with ASTM C1064/C1064M. Temperature readings were obtained using a Type K probe thermometer (Model DM-6801B). The probe was inserted to a minimum depth of 75 mm to ensure no contact with the container walls. Readings were recorded after stabilization (within 2 min).

C. Evaluation of Hardened Concrete

The specimens were demolded after 24 ± 1 h, and then placed in one of two distinct curing environments:

- Air curing: The specimens were covered with tarpaulins and moistened with water 3 times daily for 14 days, in accordance with ASTM C171 guidelines for moisture retention. This process simulates standard site curing practices, which are required by codes to limit moisture loss and early-age shrinkage cracking rather than uncontrolled drying.
- Seawater immersion: Specimens were fully immersed in natural seawater for 28 days to simulate marine service conditions.

- Compressive strength: Cubic specimens (15 cm × 15 cm × 15 cm) were cast and cured under the respective conditions. Testing was conducted for 28 days in accordance with ASTM C39/C39M.
- Flexural tensile strength: Prismatic specimens (15 cm × 15 cm × 60 cm) were evaluated after 28 days according to ASTM C78. Flexural strength was determined using a standard loading machine to identify the maximum stress at failure on the tension surface.

D. Temperature Measurement in a Mass Concrete Block

A massive concrete block measuring 500 cm × 200 cm × 120 cm was cast using a FA20SF5 mix with a plasticizer added at a rate of 0.8 l/100 kg of binder. Temperature sensors were installed at the appropriate points immediately after concrete pouring, as shown in Table II and Figure 1, and covered the measurement points. Samples for workability and compressive strength testing were taken three times: at the beginning, middle, and end of the concreting process. Mass concrete blocks and control specimens were cured in air, covered with a tarpaulin, and watered 3 times/day for 21 days. Environmental monitoring data were obtained from the Campbell weather station located in Dam Bay, Nha Trang, Vietnam.

TABLE II. ARRANGEMENT OF TEMPERATURE MEASURING POINTS

Attribute	Sensors along the radial center line (Core sensors)	Sensors located near the edge (Near-edge sensors)	Sensors located near the surface (Surface sensors)
Sensor IDs	CT1, CT2, CT3, CT4, CT5	B1, B2, B3, B4, B5, B6, B7, B8, B9, B10	S1, S2, S3, S4, S5, S6, S7, S8, S9
Distance from the top surface	60 cm	50 cm	2,5 cm
Distance from the side boundary	100 cm	50 cm	100 cm (S1, S2, S3, S4, S5); 2,5 cm (S6, S7, S8, S9)

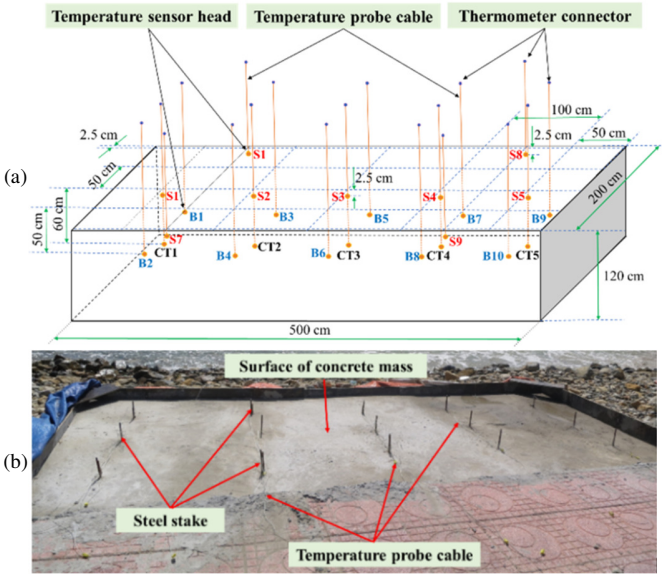

Fig. 1. Mass concrete blocks and temperature sensor locations: (a) Schematic experiment model, (b) concrete blocks after 28 days.

III. RESULTS AND DISCUSSION

A. Properties of Fresh Concrete

Figure 2 shows the variations in slump and initial temperature of concrete mixtures with different ratios of ingredients. Visual observation during slump testing revealed no significant segregation or bleeding, likely because the high fine content in the sea sand acted as a stabilizer. Post-mixing temperatures remained stable (29.9–32.6 °C), suggesting that the initial workability was not significantly affected by thermal influences. Despite the angularity often found in marine aggregates, the fine modulus of 1.1, combined with the spherical morphology of the FA, resulted in good particle packing. Therefore, the effect of temperature on workability can be considered insignificant. In contrast, slump varied significantly depending on the mix ratios and was strongly dependent on the mineral admixture content. Replacing cement with FA significantly increased the slump, especially at FA20 and FA30. This is due to the spherical shape and smooth texture of FA particles, which reduce internal friction and improve the flowability of fresh concrete. However, the addition of SF significantly decreased the slump at all replacement levels.

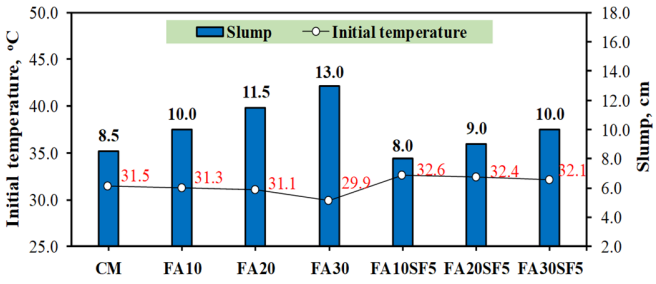

Fig. 2. Slump and initial temperature of concrete mixes.

Figure 3 shows the initial and final setting times of the studied mixes. For the control mix of CM, the initial setting time is about 572 min, and the final setting time is about 686 min. With the addition of FA at ratios of 10–30% (FA10, FA20, and FA30), both setting times gradually increase. Specifically, the initial setting time increases from 627 min to 669 min, and the final setting time increases from 739 min to 794 min, representing an increase of 10–17% compared to CM. For mixes combining FA and 5% SF (FA10SF5, FA20SF5, and FA30SF5), the initial setting time is not significantly longer than that of the CM mix, despite the fact that the initial setting time of the FA10SF5 mix is shorter (approximately 537 min). However, the final setting time increased significantly, ranging from 717 min to 771 min. Thus, the total setting time for the FA–SF group increased to approximately 160–180 min, which is significantly longer than the CM group and mixes containing only FA. The measured chloride content of the unwashed sea sand (0.06%) is at the lower end of the range of values reported for natural marine sands. This is consistent with supratidal sampling, in which rainfall and intermittent tidal flushing can reduce residual salts. Though low, this chloride level may slightly affect early hydration and setting. However, the measured setting times reflect the net balance between

potential ionic acceleration (Cl^- and SF nucleation) and the counteracting effects of FA dilution and the water-reducing admixture. From a practical standpoint, this extended setting time is advantageous for mass concrete placement to prevent cold joints, though it requires adjusted finishing schedules.

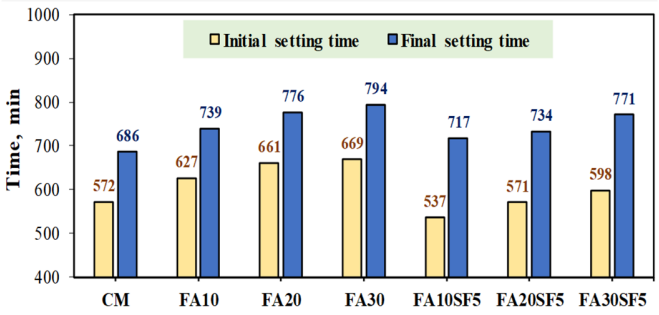

Fig. 3. Initial and final setting times of concrete mixes.

B. *Properties of Hard Concrete*

Figure 4 illustrates the compressive strength of concrete mixes under two curing conditions: air and seawater. The increase ranged from approximately 2 to 5 MPa, reflecting the combined effects of a continuous humid environment and the presence of ions in seawater. For the CM and RS specimens, the increase in strength was primarily due to maintaining optimal humidity, which facilitated a more complete hydration process. The observed strength enhancement may be attributed to accelerated early-age hydration in the chloride-rich pore solution and to the possible formation of chloride-bearing AFm phases (Friedel's salts), which can contribute to pore refinement in similar binder systems [22]. However, it is hypothesized that this chemical mechanism, combined with the physical benefits of saturation, drove the observed strength retention. In mixtures containing FA (FA10, FA20, and FA30), the difference between the two curing regimes was more pronounced because the pozzolanic reaction of FA depends heavily on humidity conditions. The seawater environment provided sufficient water to accelerate the slow hydration of FA, significantly increasing strength compared to air curing. The greatest strength gain was observed in the FA and 5% SF combinations (FA10SF5, FA20SF5, and FA30SF5). The simultaneous presence of the filling effect and SF's strong pozzolanic reaction led to the formation of a denser secondary C–S–H gel network [23]. This enhancement is likely facilitated by accelerated hydration kinetics and theorized pore filling by Friedel's salt, as observed in similar binder systems [23, 24]. Figure 5 displays the flexural tensile strength of concrete mixes after curing in air and seawater. The results show that all mixes achieved higher flexural strength in seawater, with an increase of approximately 0.3–0.9 MPa. This is consistent with the observation that submerged curing maintains a saturated state, which limits self-drying and early shrinkage, reducing matrix microcracking and allowing the hydration/pozzolanic reaction to proceed more fully [23]. For mixtures containing FA (FA10, FA20, and FA30), the flexural strength in air is lower due to dilution and the slow pozzolanic reaction rate, which leads to insufficient secondary calcium silicate hydrate (C–S–H) formation if moisture is lacking. When cured in seawater, continuous humidity helps FA react more thoroughly with $Ca(OH)_2$, creating more secondary C–S–H and purifying the capillary system while limiting cracking due to plastic shrinkage and drying. Therefore, flexural strength increases significantly for all three FA substitution levels [23, 24]. The increase in flexural strength is most remarkable for the combined group of FA and SF (FA10SF5, FA20SF5, and FA30SF5) because SF has an ultra-fine particle size, creating a filling effect and providing hydration nucleation sites, accelerating the formation of C–S–H and reducing capillary porosity at an early stage [24].

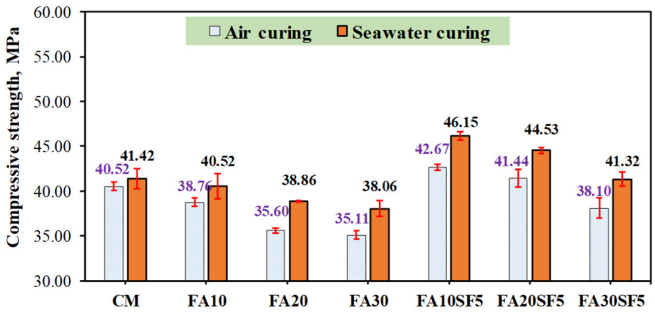

Fig. 4. Compressive strength of concrete under two curing conditions: air and seawater.

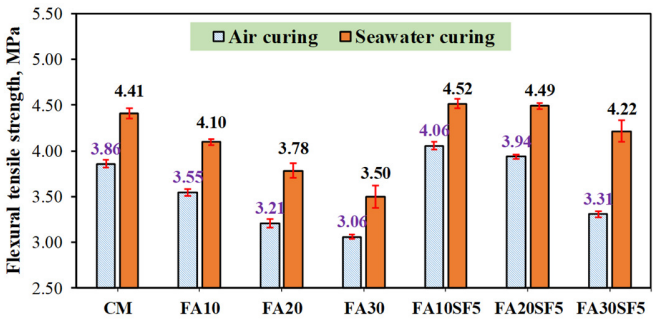

Fig. 5. Flexural tensile strength of concrete under two curing conditions: air and seawater.

C. *Characteristics of Mass Concrete Blocks*

Table III depicts the concrete mix slump and strength results after 28 days of sampling at the beginning, middle, and end of construction. The slump values varied within a very small range of 11–12 cm in both tests, with a difference of only approximately 0.5 cm across all three sampling periods. This indicates that the mix maintained its slump well with no signs of water loss or reduction in workability during transportation or construction. Regarding compressive strength (R28), the average values were 40.47 MPa (initial), 42.15 MPa (final average), and 39.14 MPa (final). The change in compressive strength during the process is negligible. Figure 6 shows the temperature change over time (i.e., age of concrete) at different locations within the concrete block. These locations include sensors in the core (CT1–CT5) and near the surface (S1–S5). The thermal profiles exhibited a characteristic three-phase evolution: a rapid exothermic stage (0–40 h) due to the high intensity of the hydration reaction in the early stages, a convective cooling stage (40–200 h) when the heat release rate

decreases and heat transfer to the environment becomes dominant, and a thermal equilibrium stage after approximately 200 h when the temperature in the block approaches the ambient temperature and fluctuates only slightly. The maximum temperature in the core (CT group) is approximately 59–60 °C after 30–35 h, whereas the near-surface region (S group) is only approximately 45–47 °C. This difference reflects the effect of heat retention in the core due to limited heat exchange conditions. In contrast, the surface experiences greater heat loss to the environment, resulting in a small, early temperature peak. The temperature difference between the core and surface peaks at approximately 12–15 °C and then rapidly decreases to 5–8 °C after 100 h, continuing to decrease, reaching 1–2 °C when the block is close to thermal equilibrium after 200 h. This study confirms that, under the proposed mix-ratio window and curing practice, hydration heat evolution in instrumented large-scale blocks remains controlled. The experimental block was unreinforced and had five faces exposed to air, resulting in faster cooling than that experienced by semi-infinite structures (e.g., dams), providing a conservative estimate of thermal gradients.

TABLE III. CONCRETE SLUMP AND 28-DAY STRENGTH BY SAMPLING TIME: START, MIDPOINT, END

Parameter	Standard	Run	Sampling time		
			Start	Midpoint	End
Slump (cm)	ASTM C143/C143M	1	11.0	12.0	11.5
		2	12.0	12.0	12.0
		Mean	11.5	12.0	12.0
Compressive strength at 28 days (MPa)	ASTM C39/C39M	1	39.07	39.51	38.84
		2	40.36	42.93	38.04
		3	42.00	44.00	40.53
		Mean	40.47	42.15	39.14

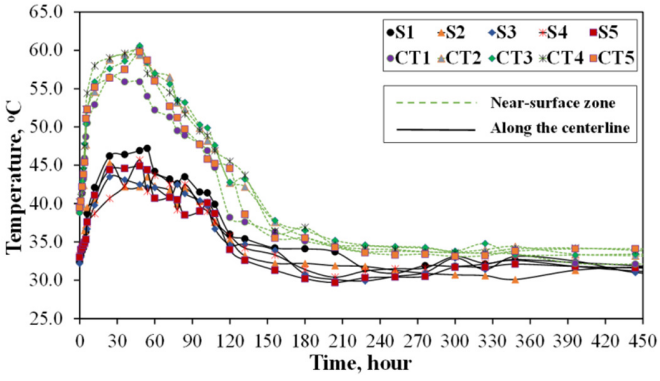

Fig. 6. Time-dependent temperature changes at the near-surface zone and along the centerline of the mass concrete block.

Figure 7 presents the temperature variation over time at different depths within the mass concrete block (Sa: near the surface, Ba: intermediate points, and CTa: core) compared to the average ambient temperature (ENa). Initially, the temperature at all depths increases sharply due to the heat of hydration. The temperature at the core (CTa) is invariably the highest, followed by Ba, while Sa is the lowest. The maximum temperature is observed within the first 30–40 h. During this time, the temperature difference between the core and the surface also reaches its maximum value, reflecting a significant temperature gradient throughout the concrete block. After this peak stage, the temperature at all locations gradually decreases and approaches a steady state. After about 150 h, the CTa and Ba temperature curves converge. Throughout the monitoring period, fluctuations in ambient temperature are reflected only in the Sa curve. This indicates that ambient temperature influence decreases with depth and that the temperature in the core region is primarily controlled by heat generated from cement hydration.

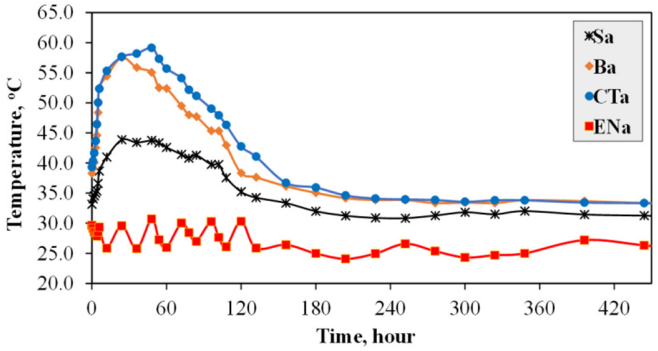

Fig. 7. Mean temperature at the near-surface zone, along the centerline of the mass, and at locations 50 cm beneath the surface.

Figure 8 shows how thermal gradients within the block change over time. Initially (0–10 h), the surface-relative gradients were: ΔT(CTa–Sa) and ΔT(Ba–Sa), surged to 13–14°C. Meanwhile, the core exhibited thermal uniformity (ΔT(CTa–Ba) < 2°C). As hydration intensified (60–120 h), the core-to-surface gradient peaked at 15–16°C, indicating that this interval was the critical window for thermal stress. However, this peak differential remained below 16°C, which is well below the typical cracking threshold of 20–25°C proposed by ACI 207 for mass concrete [25]. During this phase, the 50 cm depth functioned as a transition zone, as evidenced by the increase in ΔT(CTa–Ba) to 3–4.5 °C. By 150 h, the system approached thermal equilibrium, with internal variations dropping below 1°C (quasi-isothermal) and surface gradients stabilizing at 2–3°C. Throughout the curing process, the temperature gradients consistently followed the order ΔT(CTa–Sa) > ΔT(Ba–Sa) > ΔT(CTa–Ba). This confirms that the 10–100-h period is the primary risk window for surface cracking.

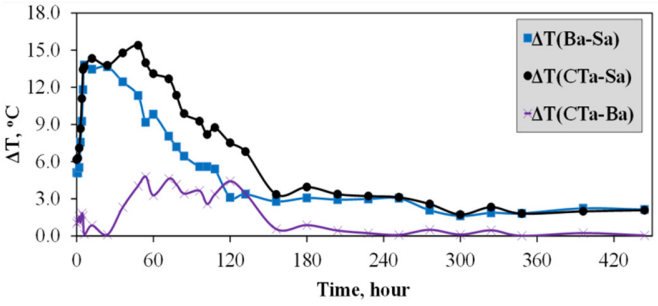

Fig. 8. Correlation of the mean temperatures measured near the surface and at a depth.

IV. CONCLUSIONS

This study validated the structural integrity and thermal safety of mass concrete produced with unwashed fine sea sand, with a fineness modulus of 1.1 and a chloride content of 0.06%. Based on experimental results from laboratory specimens and large-scale block monitoring, the following conclusions were drawn:

- Contrary to the typical degradation expected in marine environments, seawater curing yielded a compressive strength increase of up to 5 MPa, significantly outperforming air curing. This gain likely stems from synergistic marine effects: continuous moisture supports the Fly Ash (FA) pozzolanic reaction, and marine ions are theorized to accelerate hydration and facilitate pore refinement via Friedel's salt.
- The binder system demonstrated high adaptability. While replacing 10–30% of the cement with FA delayed setting times by 10–15%, incorporating 5% Silica Fume (SF) extended the final setting time. This modification effectively widened the plastic setting window from 2 h to approximately 2.5-3 h, providing a significant workability buffer for continuous mass concrete placement.
- The mixture containing 20% FA and 5% SF (FA20SF5) was identified as the optimal design, presenting an effective balance between binder efficiency and microstructural densification, delivering the highest mechanical strength across both curing conditions.
- Thermal monitoring of the 500 cm × 200 cm × 120 cm mass concrete block revealed that the chloride ions present in the unwashed sand did not cause hazardous thermal acceleration. The core temperature followed a standard three-stage hydration curve, peaking at around 60°C between 30 h and 35 h. This study provides large-scale validation of unwashed sea sand concrete, demonstrating that the accelerating effects of marine ions do not compromise the thermal performance of mass concrete when it is designed within the proposed mix and curing parameters.
- The maximum radial thermal gradient recorded was 16°C, remaining well below the standard cracking threshold for mass concrete. The thermal field stabilized within 200 h, confirming that the combination of fine sea sand and sulfate-resistant binder creates a thermally stable system suitable for large-scale coastal infrastructure.

However, this study was limited to early-age performance and did not quantify long-term reinforcement corrosion or the drying shrinkage potential of the ultra-fine aggregate. Future research could prioritize microstructural analysis and durability monitoring to fully validate the material's service life.

ACKNOWLEDGMENT

The authors express their gratitude to the Joint Vietnam-Russia Tropical Science and Technology Research Center for its support and encouragement. This research was granted by the Joint Vietnam-Russia Tropical Science and Technology Research Center (Project No. VB.Đ1.14/24).

REFERENCES

[1] M. Larik, A. Kumar, T. H. Ali, and R. Larik, "Innovative Advancements in Construction: The Sustainable Promise of Aerated Concrete Incorporating Fly Ash and River Sand," *Civil Engineering Journal*, vol. 11, no. 8, pp. 3432–3453, Aug. 2025, https://doi.org/10.28991/CEJ-2025-011-08-019.

[2] M. Bendixen *et al.*, "Sand, gravel, and UN Sustainable Development Goals: Conflicts, synergies, and pathways forward," *One Earth*, vol. 4, no. 8, pp. 1095–1111, Aug. 2021, https://doi.org/10.1016/j.oneear.2021.07.008.

[3] S. Rathnarajan and P. Sikora, "Seawater-mixed concretes containing natural and sea sand aggregates – A review," *Results in Engineering*, vol. 20, 2023, Art. no. 101457, https://doi.org/10.1016/j.rineng.2023.101457.

[4] X. L. Saleh, S. Mahmood, A. H. Hamed, and E. Zhao, "The mechanical, transport and chloride binding characteristics of ultra-high-performance concrete utilising seawater, sea sand and supplementary cementitious materials," *Construction and Building Materials*, vol. 372, 2023, Art. no. 130815, https://doi.org/10.1016/j.conbuildmat.2023.130815.

[5] J. Wang, X. Dong, C. Xu, S. Song, Q. Ren, and J. Zhu, "Influence of seawater and sea sand on early-age performance and cracking sensitivity of concrete," *Journal of Building Engineering*, vol. 79, 2023, Art. no. 107811, https://doi.org/10.1016/j.jobe.2023.107811.

[6] P. Li, W. Li, T. Yu, F. Qu, and V. W. Y. Tam, "Investigation on early-age hydration, mechanical properties and microstructure of seawater sea sand cement mortar," *Construction and Building Materials*, vol. 249, 2020, Art. no. 118776, https://doi.org/10.1016/j.conbuildmat.2020.118776.

[7] C. Zhao, Y. Li, H. Hu, and X. Shi, "Evaluation on steel corrosion risk of seawater sea sand concrete with low water-to-binder ratio by electrochemical measurement," *Construction and Building Materials*, vol. 417, 2024, Art. no. 135326, https://doi.org/10.1016/j.conbuildmat.2024.135326.

[8] J. Chen, J. Jia, and M. Zhu, "Role of supplementary cementitious materials on chloride binding behaviors and corrosion resistance in marine environment," *Construction and Building Materials*, vol. 458, 2025, Art. no. 139724, https://doi.org/10.1016/j.conbuildmat.2024.139724.

[9] U. R. Bala, R. Bhavani, and J. G. Jawahar, "Development of sustainable self-compacting concrete using slag sand and expanded clay aggregates," *Civil Engineering Journal*, vol. 11, no. 10, 2025, https://doi.org/10.28991/CEJ-2025-011-10-015.

[10] H. Ge, L. Feng, Z. Sayed, and U. Li, "Research on the performance of seawater sea-sand concrete: A review," *Construction and Building Materials*, vol. 409, 2023, Art. no. 133921, https://doi.org/10.1016/j.conbuildmat.2023.133921.

[11] T. Van Lam, N. T. Dung, D. Van Phi, V. K. Dien, and N. Van Duong, "Effects of fly ash and silica fume on properties of high-strength concrete for coastal construction," *Journal of Mining and Earth Sciences*, vol. 61, no. HTCS6, pp. 88–95, 2020, https://doi.org/10.46326/jmes.htcs2020.12.

[12] Nguyen N. T. *et al.*, "Potential using of marine sand in coastal areas of Vietnam to create concrete for rural roads," *Journal of Mining and Earth Sciences*, vol. 65, no. 6, pp. 82–89, 2024.

[13] A. P. S. Chai, M. Y. Chin, K. K. Kuok, and M. R. Rahman, "Mechanical properties of sustainable freshwater marine sand mortar," *Materials and Structures*, vol. 58, 2025, Art. no. 72, https://doi.org/10.1617/s11527-025-02571-7.

[14] M. Iqbal, D. Zhang, K. Khan, M. N. Amin, M. Ibrahim, and B. A. Salami, "Mechanical, microstructural and durability performance of seawater sea sand concrete modified with silica fume," *Journal of Building Engineering*, vol. 72, 2023, Art. no. 106583, https://doi.org/10.1016/j.jobe.2023.106583.

[15] U. Ebead, D. Lau, F. Lollini, A. Nanni, P. Suraneni, and T. Yu, "Recent advances in the science and technology of seawater-mixed concrete: A review," *Cement and Concrete Research*, vol. 152, 2022, Art. no. 106666, https://doi.org/10.1016/j.cemconres.2021.106666.

[16] U. R. Bala, R. Bhavani, and J. G. Jawahar, "Optimizing concrete mix design for cost and carbon reduction using machine learning," *Civil Engineering Journal*, vol. 6, no. 2, pp. 293–310, 2025, https://doi.org/10.28991/HEF-2025-06-02-04.

[17] M. Chen, J. Jia, and J. Zhu, "Development of admixtures for seawater sea sand concrete: A critical review on hardening, chloride penetration and steel corrosion," *Construction and Building Materials*, vol. 411, 2024, Art. no. 134219, https://doi.org/10.1016/j.conbuildmat.2023.134219.

[18] A. Panchanathan and A. Paramasivam, "Feasibility study on the use of sea sand as partial replacement of fine aggregate in concrete," *Materials Today: Proceedings*, vol. 65, pp. 468–471, 2022, https://doi.org/10.1016/j.matpr.2022.03.016.

[19] M. M. Rafi, M. A. Bhutto, and T. Aziz, "Strength and durability characteristics of concrete mixes made with unwashed sea sand as fine aggregates," *Advances in Civil Engineering Materials*, vol. 11, no. 1, pp. 321–338, 2022, https://doi.org/10.1520/acem20210139.

[20] C. S. Cai, Y. Tao, Y. Xuan, D. Zhu, and X. Poon, "Effects of seawater on Friedel's salt formation and mechanical properties associated with tricalcium aluminate," *Cement and Concrete Research*, vol. 174, 2023, Art. no. 107340, https://doi.org/10.1016/j.cemconres.2023.107340.

[21] *C143/C143M-12 Standard Test Method for Slump of Hydraulic-Cement Concrete*. West Conshohocken, PA, USA: ASTM International, 2020.

[22] *C1064/C1064M-17 Standard Test Method for Temperature of Freshly Mixed Hydraulic-Cement Concrete*. West Conshohocken, PA, USA: ASTM International, 2023.

[23] D. Pan, S. A. Yaseen, K. Chen, D. Niu, C. K. Y. Leung, and Z. Li, "Influence of seawater and sea sand on mechanical and microstructural properties of concrete," *Journal of Building Engineering*, vol. 42, 2021, Art. no. 103006, https://doi.org/10.1016/j.jobe.2021.103006.

[24] A. Arshad, M. T. Ahmad, S. Khitab, and A. Hanif, "Synergistic use of fly ash and silica fume to produce high-strength self-compacting cementitious composites," *Crystals*, vol. 11, no. 8, 2021, Art. no. 915, https://doi.org/10.3390/cryst11080915.

[25] *207.1R-05 Guide to Mass Concrete*. Farmington Hills, MI, USA: ACI Committee, 2005.